DOI: 10.1002/ejic.201100331

A Crystallographic and Mo K-Edge XAS Study of Molybdenum Oxo Bis-, Mono-, and Non-Dithiolene Complexes – First-Sphere Coordination Geometry and Noninnocence of Ligands

Prinson P. Samuel,[a] Sebastian Horn,[b] Alexander Döring,[a] Kajsa G. V. Havelius,[b] Stefan Reschke,[c] Silke Leimkühler,[c] Michael Haumann,*[b] and Carola Schulzke*[d]

Keywords: Molybdenum / Enzyme models / X-ray absorption spectroscopy / Noninnocence / Bioinorganic chemistry

Ten square-based pyramidal molybdenum complexes with different sulfur donor ligands, that is, a variety of dithiolenes and sulfides, were prepared, which mimic coordination motifs of the molybdenum cofactors of molybdenum-dependent oxidoreductases. The model compounds were investigated by Mo K-edge X-ray absorption spectroscopy (XAS) and (with one exception) their molecular structures were analyzed by X-ray diffraction to derive detailed information on bond lengths and geometries of the first coordination shell of molybdenum. Only small variations in Mo=O and Mo–S bond lengths and their respective coordination angles were observed for all complexes including those containing $Mo(CO)_2$ or $Mo(\mu\text{-}S)_2Mo$ motifs. XAS analysis (edge energy) revealed higher relative oxidation levels in the molybdenum ion in compounds with innocent sulfur-based ligands relative to those in dithiolene complexes, which are known to exhibit noninnocence, that is, donation of substantial electron density from ligand to metal. In addition, longer average Mo–S and Mo=O bonds and consequently lower ν(Mo=O) stretching frequencies in the IR spectra were observed for complexes with dithiolene-derived ligands. The results emphasize that the noninnocent character of the dithiolene ligand influences the electronic structure of the model compounds, but does not significantly affect their metal coordination geometry, which is largely determined by the Mo(IV) or (V) ion itself. The latter conclusion also holds for the molybdenum site geometries in the oxidized Mo^{VI} cofactor of DMSO reductase and the reduced Mo^{IV} cofactor of arsenite oxidase. The innocent behavior of the dithiolene molybdopterin ligands observed in the enzymes is likely to be related to cofactor–protein interactions.

Introduction

Molybdenum-dependent oxidoreductases are ubiquitous in nature and play indispensable roles in carbon, nitrogen, and sulfur metabolism in nearly all organisms from ancient archaea to human beings.[1–7] Based on structural properties and sequence homologies, these enzymes are classified into three groups:[1] xanthine oxidase (XO), sulfite oxidase (SO), and DMSO reductase (DMSOR). The XO and SO families bear one characteristic molybdopterin (mpt) ligand at the molybdenum cofactor (Moco), whereas in the DMSOR family molybdenum is bound to two mpt units (Figure 1). Structural information has been obtained by X-ray diffraction (XRD) for numerous Moco enzymes[8–9] revealing the distinct molybdenum coordination environment in many

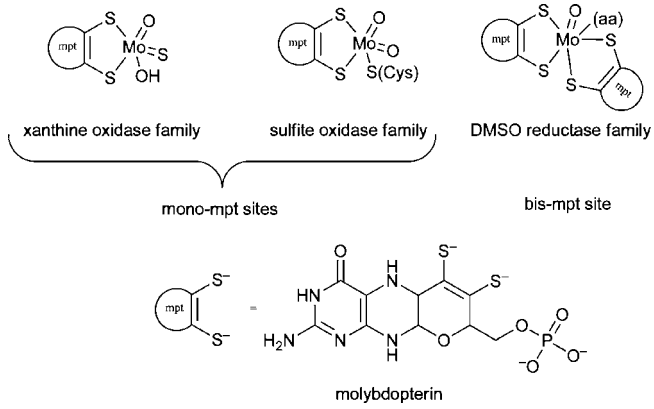

Figure 1. Structural representations of the active sites of molybdenum/molybdopterin-dependent enzymes. In the SO family the coordinated amino acid is cysteine, in the DMSOR family the amino acid can be serine, cysteine, selenocysteine, or aspartate. In the XO type enzymes no amino acid coordination has been observed.

[a] Georg-August-Universität Göttingen, Institut für Anorganische Chemie,
Tammannstr. 4, 37077 Göttingen, Germany
[b] Freie Universität Berlin, Institut für Experimentalphysik,
Arnimallee 14, 14195 Berlin, Germany
E-mail: michael.haumann@fu-berlin.de
[c] Universität Potsdam, Institut für Biochemie und Biologie, Molekulare Enzymologie,
Karl-Liebknecht Strasse 24-25, 14476 Potsdam, Germany
[d] Trinity College Dublin, School of Chemistry, College Green, Dublin 2, Ireland
E-mail: schulzkc@tcd.ie
Supporting information for this article is available on the WWW under http://dx.doi.org/10.1002/ejic.201100331.

cases. However, monitoring changes to the active site crystallographically, for instance oxidation, reduction, substrate binding, and so on, as they occur is difficult at best. Quite often such manipulation results in disintegration of the crystals, and crystallography provides a rather static picture of the active site. For unraveling the catalytic mechanism involving structural changes at the molybdenum site in intermediates, XAS at the Mo K-edge is a valuable tool.[10–21]

The mpt ligand coordinates to the molybdenum active site by its dithiolene function (Figure 1). In principle, this functional group is able to participate in redox reactions by donating electrons to the metal center.[22–24] To that effect, the formal oxidation state of molybdenum does not necessarily reflect the electronic situation of the complex accurately. The actual relative oxidation level of a metal, that is, the oxidation state of the metal relative to that of a complex with a known oxidation state or one that is less ambiguous due to its structure, can be readily determined from the relative positions of the metal K-edge XAS spectra on the energy scale.[25–34] Determining Mo–Sulfur and Mo–oxo bond lengths even reveals aspects of the first-sphere coordination geometry in some cases.[15] In addition, the second coordination shell may influence the electronic structure of the metal site, for example, covalence of the metal–ligand bonds.[35] However, Mo K-edge XAS data for model complexes for comparison with Moco enzymes are surprisingly rare. Therefore, the aims of this study are to elucidate the ability of XAS to detect subtle differences in the molybdenum coordination in model compounds with electronically distinct dithiolene ligands (aromatic, nonaromatic, pyran–dithiolene) and to provide a collection of XAS Moco model data. The combination of crystallographic, XAS, and IR spectroscopic methods is further expected to provide detailed information on how particular ligands affect the electronic structures and coordination geometries of the molybdenum complexes in comparison with the active sites of Moco enzymes.

The broad class of model compounds, to which most of the complexes investigated here belong, was developed soon after structural information about the Moco active sites became available.[1–9] Numerous molybdenum compounds with two dithiolene ligands have been reported, which model the bis-mpt active site of enzymes from the DMSOR family, that is, DMSOR itself and, more accurately, arsenite oxidase (AO).[36–44] The coordinating amino acid residue, commonly found in the DMSOR family, is replaced by one terminal oxo ligand in AO.[45–46] In this work, both newly developed and previously known model compounds were investigated and compared. These compounds can be classified into three groups: i) six mono-oxo bisdithiolene Mo complexes resembling the active site of AO, ii) three models in which one or both of the dithiolene ligands have been replaced by an innocent bidentate sulfur-only ligand (S_4^{2-}), which mimics aspects of the mono-mpt SO, and (iii) one compound with a $Mo(\mu\text{-}S)_2Mo$ motif and one dithiolene ligand on each of the molybdenum centers. The coordination spheres are completed by oxo (Mo=O), sulfido (Mo=S) or carbonyl [$Mo(CO)_2$] ligands.

For nine of the ten compounds, crystallographic data were either available from the literature or newly determined. All ten compounds were investigated by XAS and FTIR spectroscopy. Cogent correlations were observed between the Mo=O and Mo–S bond lengths, the Mo=O FTIR stretching frequencies, and the apparent molybdenum oxidation level. This suggests that even readily available IR data, at least for model compounds, may be able to provide an insight into electronic properties that goes beyond merely assessing the Mo=O bond strength. The results emphasize the pronounced noninnocent character of dithiolene ligands compared to the innocent sulfide-based systems in the models. Comparison of the structural data of the models with the properties of the bis-mpt Moco species in AO and DMSOR enzymes reveals that in both cases the molybdenum geometry appears to be largely dominated by the molybdenum ion itself. The apparent innocent behavior of mpt in the enzymes may therefore reflect significant protein–cofactor interactions, possibly including the influence of amino acid coordination to molybdenum.

The ten model compounds investigated were chosen for distinct reasons. Their common characteristic is the presence of four sulfur donors in the equatorial plane of the square-based pyramidal or octahedral coordination geometry. Variations in the models include the functional groups these sulfur donors are part of, the coordination geometry, mono- or binuclearity, formal oxidation state of molybdenum, the presence or absence of an apical oxo ligand, the aromaticity or nonaromaticity of the dithiolene ligand system, and variation of the dithiolene substitution pattern. Some of the components are frequently used starting materials in our labs and others were prepared specifically for this study. The variety of the chemical structures allows us to assess the influence of the character of the sulfur donor ligand on the geometric and electronic situation at the molybdenum center and the apical oxo ligand, the influence of the oxygen atom and the coordination number on the Mo–S bond lengths, and the influence of steric restraints on the molybdenum center.

Results

Model Compound Synthesis and Crystallography

Noninnocence of dithiolene ligands is commonly associated with electron donation towards a metal center, which alters not only the metal–sulfur, but also the sulfur–carbon and even C=C bonds.[47] In molybdenum-dependent oxidoreductases such effects may be expected to be pronounced for oxidized Mo^{VI} states of the active site and less relevant for Mo^{IV}. However, in contrast to dithiolene model compounds, mpt generally seems to be innocent in the enzymes.[4] In order to investigate how a variation of the degree of noninnocence of the ligands affects the electronic and structural properties around the metal center, ten molybdenum complexes with and without dithiolene ligands were prepared either according to literature procedures or

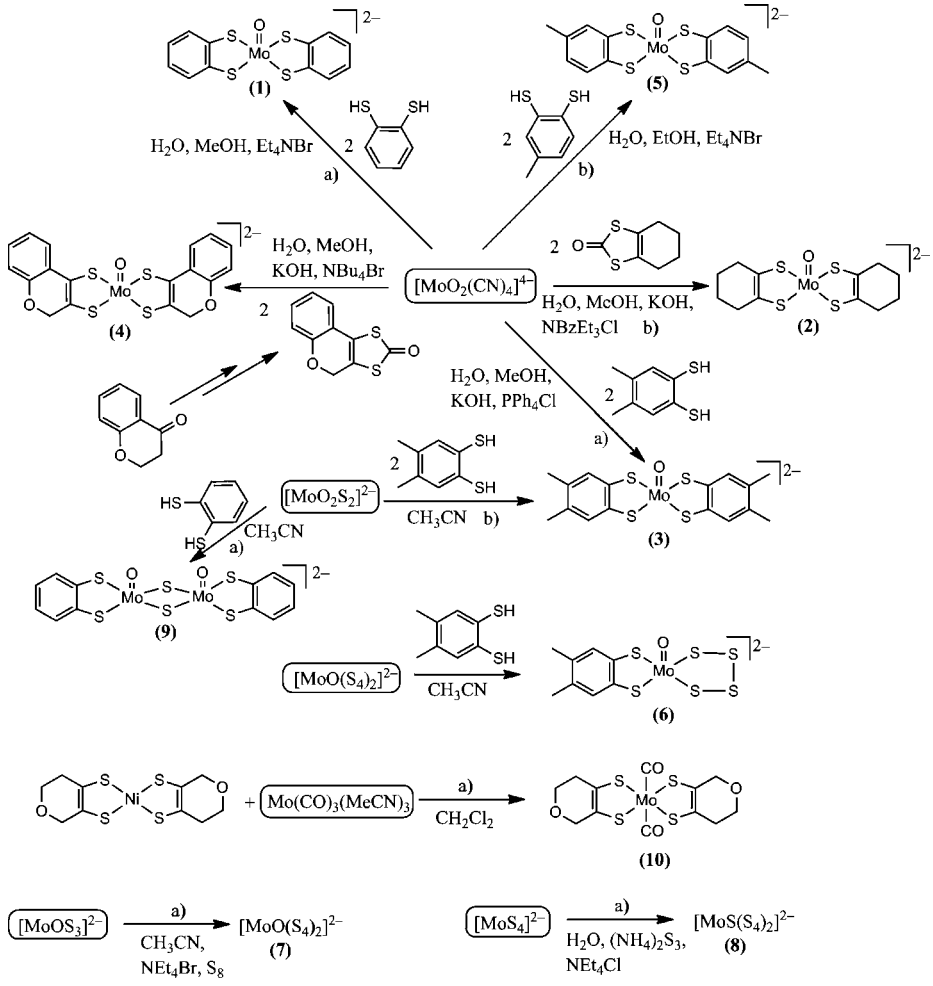

Scheme 1. Synthetic procedures for the ten molybdenum complexes. (a) compounds were synthesized according to literature procedures.[20,37,42–43,50,52] (b) compounds are known in the literature, but modified methods were used for their preparation.[42,52–53]

by synthetically straightforward combinations of molybdenum precursors with the respective ligands (Scheme 1).

Except for the binuclear complex **9**, bearing two Mo^{V} cores, all centers are in the formal Mo^{IV} oxidation state. Among these ten compounds, two are entirely new (**4** and **6**). Compound **6**, $[NEt_4]_2[MoO(xdt)(S_4)]$, is the product of a reaction between equimolar amounts of $[NEt_4]_2[MoO(S_4)_2]$ and the dithiolene ligand. To the best of our knowledge this is the most economic and straightforward procedure for the synthesis of a molybdenum monodithiolene compound reported so far. Compound **4** with a dithiolene ligand similar to mpt was prepared based on a modified method.[48–50] The syntheses[42,44,51–53] and crystal structures[42,44] of cyclohexenedithiol **2** and toluenedithiol **5** have been reported before. In this study, modified and more economic methods for their preparation were employed. For **2** a different cation than that in the published study[42] was used and consequently the space group of the crystal structure is not the same. *R* values and standard deviations of bond lengths are smaller than those for the published structure and additional bond lengths and angles are now reported (Table 1). One cyclohexene ring carbon atom of one of the dithiolene ligands in **2** is disordered and appears in two positions, but the immediate coordination sphere of molybdenum is unaffected by this. The crystal structure of **5** is quite similar to that published. However, the Mo–S bond lengths are slightly different and more precisely determined in the new low temperature structural analysis. In addition, the disorder of the anions (enantiomeric, i.e. rotameric, molecules are located on the same position) is much less pronounced (80% of the major species vs. 60% previously). Diffracting crystals of **6** were quite thin and the measuring time was long. Towards the end of the measurement ice crystals formed around the sample leading to a high internal *R* value of 0.1219, which is not a structural but rather a measurement issue. Complex **4** carries two dithiolene ligands, which, in addition to the functional group coordinating molybdenum, contain the pyran ring of mpt. The crystal structure of **4** is a rare example in which the *cis*-isomer crystallized instead of the usually physically favored *trans*-isomer with respect to the orientation of the unsymmetrical ligands towards each other. The two tetrabutylammonium cations were found as separate molecules in the asymmetric unit of **4** and both were slightly disordered with

respect to one methyl group each. The crystallographic collection and refinement data for the four X-ray structure analyses are summarized in the Experimental Section.

Structural Features of the Complexes from XRD and XAS

The relevant crystallographic metric parameters of the first coordination shell around molybdenum in the models are summarized in Table 1. Data for **1**, **3**, **7**, **8**, and **9** were taken from the literature. In addition, data for the enzymatic paragon for most of the model compounds, AO, is listed. X-ray structural data is unavailable for **10**. All compounds in the present crystallographic study (**2**, **4**, **5**, **6**, Figure 2) and the previously published structures (**1**, **3**, **7**, **8**, **9**), exhibit a distorted pyramidal coordination geometry with four sulfur donors in the basal positions and molybdenum raised slightly above this plane in the direction of the apical ligand. Remarkably few structural differences are observed in the complexes with different dithiolene ligands. The binding situation appears to be dominated by the dithiolene function and the molybdenum ion itself without much influence of the dithiolene substituents. Notably, even exchange of the noninnocent sulfur donors for innocent ligand systems does not change the geometry considerably.

Table 1. Bond lengths [Å] and angles [°] of the first coordination shell around molybdenum from crystal data. Data for **1**, **3**, **7**, **8**, **9**, and AO were taken from the literature.

	1[37]	**2**	**3**[20]	**4**	**5**	**6**	**7**[43][a]	**8**[54][b]	**9**[55][c]	AO[45]
Mo=O[1]	1.689[I]	1.712(2)	1.735(11)	1.694(5)	1.697(3)	1.694(2)	1.685(7)		1.699(2)	1.61
Mo=O[2]	1.700[II]								1.784(2)	
Mo–S1 (shortest)	2.379[I]	2.3735(9)	2.304(2)	2.383(2)	2.3745(16)	2.3191(8)	2.363(2)	2.331(1)	2.3329(9)	2.31
Mo–S2	2.384[II]	2.3754(9)	2.394(2)	2.392(2)	2.3870(15)	2.3757(8)			2.3364(9)	2.36
Mo–S3	2.387[I]	2.3817(10)	2.435(2)	2.399(2)	2.3884(15)	2.3998(8)			2.4055(8)	2.38
Mo–S4 (longest)	2.391[II]	2.3868(11)	2.498(2)	2.399(2)	2.3893(16)	2.4120(8)	2.395(2)	2.387(1)	2.4175(8)	2.39
Mo–S (average)	2.383[I] 2.388[II]	2.3794	2.408	2.393	2.3848	2.3766	2.379	2.359	2.3730	2.36
Δ (Mo–S)[d]	0.008[I] 0.007[II]	0.0133	0.194	0.016	0.0148	0.0929	0.032	0.056	0.0846	0.08
O=Mo–S1	106.95[II]	107.17(8)	108.8(4)	106.3(2)	107.72(13)	109.46(8)	110.62(17)	110.83(3)	110.50(9)	
O=Mo–S2	107.86[I]	109.35(8)	107.8(3)	109.4(2)	108.44(13)	107.86(7)			109.19(8)	
O=Mo–S3	108.70[I]	107.31(8)	109.5(3)	109.0(2)	106.48(13)	106.78(8)			103.20(9)	
O=Mo–S4	109.41[II]	111.38(8)	108.8(4)	107.4(2)	107.34(13)	107.48(7)	106.77(17)	105.88(3)	105.67(8)	
O=Mo–S (average)	108.28[II] 108.18[I]	108.80	108.7	108.0	107.50	107.90	108.70	108.36	107.14	
Δ (O=Mo–S)[e]	0.84[I] 2.46[II]	4.21	1.7	3.1	1.96	2.68	3.85	4.95	7.3	
Mo=S								2.128(1)		

[a] Due to symmetry only two distinct values exist for these angles and distances. [b] Values given are for S=Mo–S not for O=Mo–S and due to symmetry only two distinct values exist for angles and distances. [c] Data for Mo–S distances and O=Mo–S bond angles are mean values for both Mo centers. [d] Difference between longest and shortest Mo–S bonds. [e] Difference between largest and smallest O=Mo–S angles. I and II refer to the two different anions found in **1**.

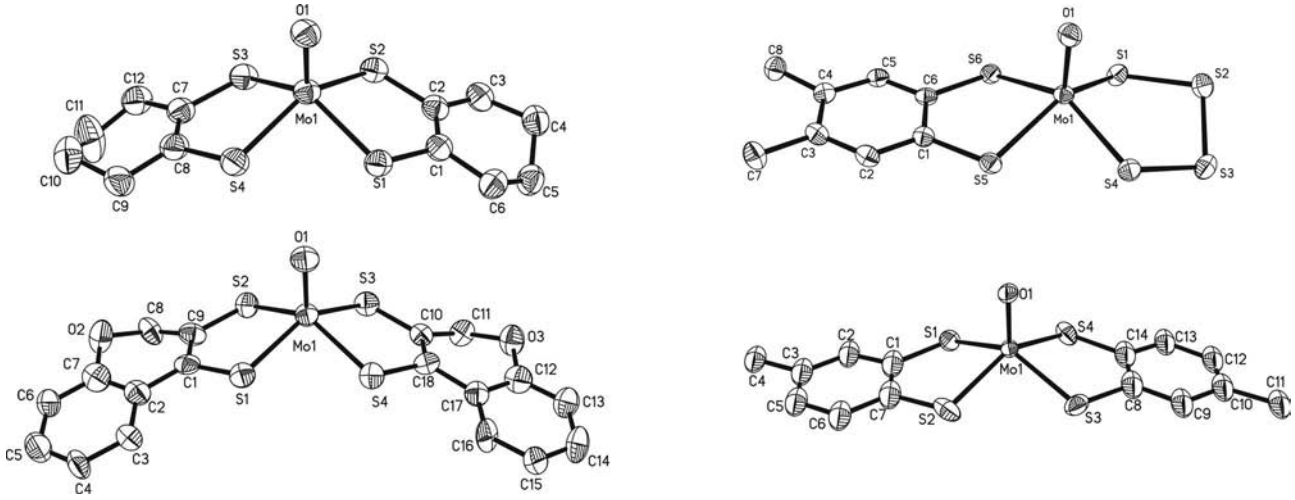

Figure 2. Molecular structures of **2** (top left), **6** (top right), **4** (bottom left), and **5** (bottom right). Thermal ellipsoids are shown at 50% probability. H atoms are omitted for clarity. In **2** the carbon atom C10 is disordered over two positions; only one position is shown here. For **5** only the major (80%) of the two cocrystallized isomers is shown (left or right handed twofold rotation axis along the Mo=O bond).

Classifying the model complexes into three groups, (i) those with two dithiolene ligands (**1**, **2**, **3**, **4**, **5**), (ii) those with one or two innocent sulfur-based ligands (**6**, **7**, **8**), and (iii) that with a $Mo(\mu S)_2Mo$ motif (**9**), facilitates a more detailed evaluation of their characteristic features. Carbonyl species **10**, for which no crystallographic data is available, is treated separately.

Extended X-ray absorption fine structure (EXAFS) analysis was employed to derive structural parameters of the molybdenum sites in powder samples of the models similar to the noncrystalline samples used for FTIR spectroscopy and for the DMSOR protein (see below). Figure 3 shows the Fourier transforms (FTs) of the EXAFS spectra and simulation curves of representative members of the three groups of models. Complex **3** represents the bisdithiolene group. Its two FT peaks reflect the typical Mo=O and Mo–S distances (Figure 3). Complex **7** represents the group with innocent sulfur-based ligands. In its FT spectrum a third peak caused by the sulfur atoms in the second coordination sphere of Mo is observed (Figure 3). Complex **9** shows a pronounced FT feature due to the Mo–Mo distance (Figure 3), which was determined to be 2.891 Å by XRD and 2.89 Å by EXAFS. The FT spectrum of **10** showed peak features at small distances due to contributions from the carbonyl ligands (Figure 3). EXAFS analysis revealed almost two Mo–C(=O) bonds (2.04 Å) and four Mo–S bonds (mean length 2.37 Å) (Table 2 and Table S1), in agreement with the anticipated structure of **10** (Scheme 1). A Mo=O bond with low coordination number was found to improve the EXAFS fit quality (Table S1), pointing to the replacement of CO by O in a fraction of the EXAFS sample of **10**.

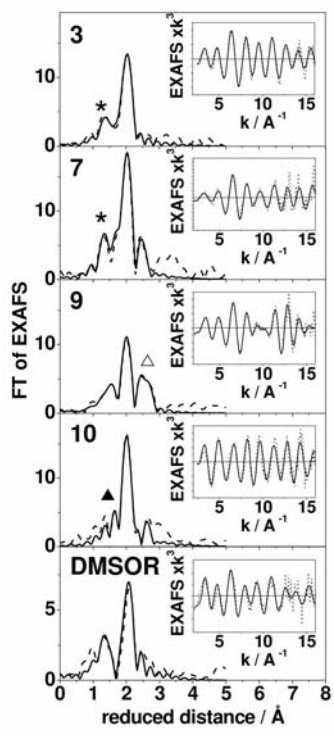

Figure 3. FTs of EXAFS spectra (inset) of Mo complexes representing the bisdithiolene **3**, innocent sulfur-based ligand **7**, binuclear **9** groups, and the dicarbonyl **10** in comparison to oxidized DMSOR. Dashed lines, experimental data; solid lines, simulations with parameters in Table 2 and S1. FTs were calculated for *k*-values up to 16 $Å^{-1}$ and using $\cos^2$ windows extending over 10% at both *k*-space ends. FT features due to Mo=O **3** and **7** (*), Mo–C(=O) **10** (▲), and the Mo–Mo distance in **9** (Δ).

As mentioned above, all crystallographically characterized compounds exhibit the same slightly distorted square-pyramidal geometry around molybdenum. In the bisdithiolene group, the two 1,2-benzenedithiolate ligands (bdt) of **1** are modified by removing the aromaticity in **2** and by the addition of methyl groups in **5** (one per ring) and **3** (two per ring), whereas **4** contains biomimetic pyran rings. In the case of **1**, two complex anions (I and II in Table 1) are present in the asymmetric unit of the crystal structure,[37] but for both molecules due to symmetry only two instead of four different Mo–S bond lengths and angles were found per anion, giving a total of four distinct values for all eight Mo–S bonds and oxo–molybdenum–sulfur angles. The precision of the mean Mo–S distance is 0.001 Å for the crystallographic data, that is, considerably smaller than the observed difference between the longest and the shortest Mo–S bond of 0.008 Å in each anion (Table 1). The longest Mo–S distance (2.391 Å) correlates with the largest O–Mo–S angle (109.41°) and with the longer Mo=O (1.700 Å) bond of the two molecules. XAS analysis reveals that the sample of **1** was partially oxidized, judged from its considerably high K-edge energy (see below). This, and an additional Mo–O distance at ca. 2.1 Å in about 50% of the molecules detected in the EXAFS simulation (Table S1), suggested a fraction of six-coordinate Mo^{VI} in the XAS

Table 2. EXAFS-derived interatomic distances [Å] and Mo K-edge energies [eV] for complexes **1**–**10**, oxidized DMSOR containing Mo^{VI}, and reduced AO containing Mo^{IV}. For complete sets of EXAFS fit parameters see Supporting Information (Table S1).

	Oxo bisdithiolene complexes					Mo^V	$Mo–S_4$ complexes			Mo–CO	Enzymes	
	1	**2**	**3**	**4**	**5**	**9**	**6**	**7**	**8**	**10**	DMSOR	AO[a]
Mo=O	1.711	1.720	1.706	1.717	1.708	1.705	1.702	1.680	1.697[b]		1.717	1.734
Mo–X						2.885[c]			2.154[b][d]	2.038[e]	1.975[f]	
Mo–S	2.396[g]	2.374	2.392	2.390	2.392	2.363	2.393[g]	2.373	2.374	2.367	2.468[g]	2.367
$E_{edge} - 2 \times 10^4$	12.91	12.16	11.89	11.84	11.75	11.98	11.79	12.06	11.99	12.01	13.77	

[a] Values were taken from ref.[46] [b] Coordination numbers of $N_{(Mo=O)} = 0.5$ and $N_{(Mo=S)} = 0.5$. [c] Mo–X denotes Mo–Mo. [d] Mo–X denotes Mo=S. [e] Mo–X denotes Mo–C(=O). [f] Mo–X denotes Mo–O(H). [g] Average values for two S shells. Other Mo–S bond lengths were derived by using a single S shell in the EXAFS simulations (Table S1). For the Debye–Waller parameters used in the EXAFS fits, see Table S1.

sample. As the complex was synthesized and characterized by mass spectrometry and elemental analysis directly prior to preparing the XAS sample, this observation points to oxidation during sample handling. However, the 1.71 Å Mo=O distance from EXAFS is close to the average of the two Mo=O distances of both anions in the crystal structure.

The addition of one methyl group to bdt in **5** does not significantly affect the first Mo coordination sphere (Table 1). In contrast, the addition of two methyl groups per bdt in **3** results in the longest Mo=O bond observed (1.735 Å) and a wider spread of the four Mo–S bond lengths (ΔR = 0.194 Å) in the crystal data.[21] It must be noted, that the structure of **3** involves two disorder problems. Firstly the tetraethylammonium cation (TEA; one independent molecule in the asymmetric unit) is substantially disordered with three arms appearing in two positions and one arm in three positions. Secondly the complex anion is disordered with the Mo=O moiety mirrored across the S4-plane made by the four sulfur donors of the two dithiolene ligands. Accordingly, the precision of the structural data of the first coordination shell around Mo is not as high as for most of the other crystal structures, but the error is still smaller than the observed differences in the relevant bond lengths and angles. In this case the sulfur atom furthest from Mo is not involved in the largest O=Mo–S angle, which means that the elongation of this bond is not due to the *trans* influence of the oxo ligand. The increased average Mo–S and Mo=O bond lengths compared to **1** and **5** are partly based on the disorder across the S4 plane, but also on the proximity of one disordered arm of TEA to the oxo ligand, indicating some kind of interaction (H-bonding) between the oxygen atom and the methyl protons. This bond length difference cannot be observed to the same extent in the EXAFS data (Table 2). The respective distances are very similar in **3** and **5** with only a slight tendency for longer Mo–S bonds in **3** and they are longer than those in **1**. The discrepancy between EXAFS and the crystal data is most likely due to different packing of molecules in the crystalline and XAS powder samples. Comparing only **1** and **3**, the results are in agreement with the chemical composition of both. The two methyl groups of **3** with their positive inductive effect increase the electron density of the aromatic system and consequently that of the dithiolene moiety. Due to the delocalization of the double bonds, however, this results not in better donation into the Mo–S bonds but in the promotion and partial occurrence of C=S bonds (giving rise to electron donation to the metal center), with increased Mo–S bond lengths visible both in the EXAFS and XRD derived distances. The "intermediate" **5** in the case of XRD is more similar to **1** and in the case of XAS more similar to **3**, indicating that for asymmetrically substituted dithiolene compounds, intermolecular interactions have a more marked effect on structural features than for symmetric species, depending on the solid state of the sample.

In the crystal structure of **2** the average Mo–S distance is slightly smaller than those in **1** (both molecules), **3**, and **5** containing aromatic dithiolene ligands, whereas the Mo=O bond is longer. The two nonaromatic dithiolene ligands in **2** are able to form stronger bonds with molybdenum by stronger electron donation into these bonds, without involving the thione form of the ligand, which in turn decreases the electron donation from the apical oxygen and weakens the Mo=O bond.[42] The two dithiolene ligands of **4** contain the pyran ring of mpt (Scheme 1, Figure 1, and Figure 2). For **4** the crystallographic difference between the longest and the shortest Mo–S bond is in the range of **1** and **2**, but smaller than for **3**, as are the differences for the O=Mo–S angles. The average Mo–S distance is at the longer end of the range compared to the other complexes, indicating that the donation of electron density into this bond is less pronounced, though this does not affect the Mo=O bond, which is in the typical range. The distances in the first coordination sphere of molybdenum from XRD and EXAFS data are comparable (Table 1 and Table 2) and without any significant distinctions.

Complexes **7** and **8** have only innocent sulfur-based ligands and no dithiolene ligand. The two shorter (2.36 Å and 2.31 Å) and two longer (2.35 Å and 2.39 Å) Mo–S single bonds in the crystal structure cannot be resolved in the EXAFS data, but the average Mo–S distances from EXAFS are similar to those from XRD (Table 2). The values for the Mo–S distances and O/S=Mo–S angles of **7** and **8** are not exceptionally different from those with the dithiolene group, but the spread in the Mo–S bond lengths is larger. This highlights the higher coordination flexibility of the innocent sulfur donors without any double bonds compared to the dithiolenes. In **6**, one of the dithiolene ligands of **3** is exchanged for the same bidentate tetrasulfide that is already part of the metal precursor. The Mo–S bonds to the tetrasulfide ligand are shorter than those to the dithiolene ligand, again emphasizing an increased coordination flexibility and subsequently a better orbital overlap. The largest O=Mo–S angle correlates with the shortest Mo–S distance, suggesting that steric restraints are more important for the observed bond lengths than the electronic structure of the complex.

Compound **9** contains two Mo^{V} centers that are bridged by two sulfides, in principle providing a similar coordination sphere as that in **6**, but with considerably less flexibility. The crystal structure of **9** (Table 1) reveals two shorter and two longer Mo–S bonds similar to **6**. However, compared to **6** the angular differences in **9** are much more pronounced due to the increased rigidity. Remarkably, the higher oxidation state does not have an apparent impact on the complex geometry, in contrast to the geometrical change observed in oxidized bisdithiolene complexes.[56–57] EXAFS analysis provides similar, but slightly smaller metrical values for the average Mo–S and M=O bond lengths.

EXAFS-derived values for the Mo=O bond (1.73 Å) and the average Mo–S distance (2.37 Å) of reduced AO[46] (Table 2) are similar to the respective bond lengths in its crystal structure[45] and agree well with the values of the bisdithiolene models, in particular nonaromatic **2**. Oxidized DMSOR from *R. capsulatus* provides an example of an octahedral Mo^{VI} site. The present EXAFS analysis (Figure 3) reveals one Mo=O bond (1.72 Å), one Mo–O(Ser) bond

(1.97 Å), and one longer Mo–S (2.59 Å) and three shorter Mo–S (2.43 Å) bonds (Table 2 and Table S1). These values are similar to previously published average distances from EXAFS analysis of oxidized DMSOR.[10,58–59] The difference in the two Mo–S shell distances, determined by EXAFS to be 0.15 Å, is similar to that found from XRD analysis of DMSOR,[60–62] which shows that the longer Mo–S bond of one mpt is located opposite the oxo ligand, as expected.

Metal–Ligand Bond Lengths, ν(Mo=O), and Molybdenum Oxidation Level

Figure 4A shows a plot of the Mo=O bond lengths (from EXAFS and XRD) vs. the stretching mode frequencies of the oxo group [ν(Mo=O)] from FTIR spectroscopy for the molybdenum complexes **1**–**7** and **9** (**8** and **10** do not bear oxo ligands). Notably, the correlation is decidedly better for the EXAFS-derived Mo=O bond lengths than for the crystallographic data. This is most likely based on the use of similar (amorphous or microcrystalline) powder samples in the XAS and FTIR measurements. Notably, sample preparation for both methods involves extensive grinding of compounds, dilution in a different solid compound and pressing of pellets. In the crystalline samples, crystal forces and packing effects can have a profound influence on the Mo=O bond length, which is particularly exposed to intermolecular contacts and interactions through the doming of the Mo=O moiety above the S4 plane. Bulk material, however, is very often not crystalline. Even if the material is microcrystalline its surface area is considerably larger than in crystals of sufficient size for X-ray diffraction experiments and consequently the proportion of molecules that are not only exposed to crystal forces but to the environment as well is significantly larger. This emphasizes the ability of EXAFS to provide more congruent data for comparison with other bulk spectroscopy techniques and a more reliable insight into the properties of the respective material.

Complexes in which the dithiolene ligands dominate the metal coordination sphere tend to show longer Mo=O bonds and consequently lower ν(Mo=O) values, whereas for those with innocent sulfur-based ligands (**6**, **7**) the opposite is true (Figure 4A). This emphasizes the superior ability of dithiolene ligands to donate electron density to molybdenum compared to innocent sulfur donor ligands. An increase in electron donation to the central metal by the four dithiolene sulfur atoms decreases electron donation from the oxo ligand, consequently elongating this bond.

The formal oxidation state of all complexes investigated, except binuclear Mo^{V} **9**, is Mo^{IV}. The K-edge energies as determined from X-ray absorption near edge structure (XANES) spectra of the complexes are around 20012 eV and actually in agreement with the average Mo^{IV} oxidation level[63] (Table 2). For **1** the edge energy is about 1 eV higher due to approximately 50% oxidation to the Mo^{VI} level, in agreement with the EXAFS analysis. In general, complexes with dithiolene ligands show longer Mo=O and Mo–S bonds and lower edge energies than complexes containing innocent sulfur-based ligands. Again, a correlation for the latter proves to be better for the EXAFS-derived distances than for the XRD data (see Figure 4B). The X-ray absorp-

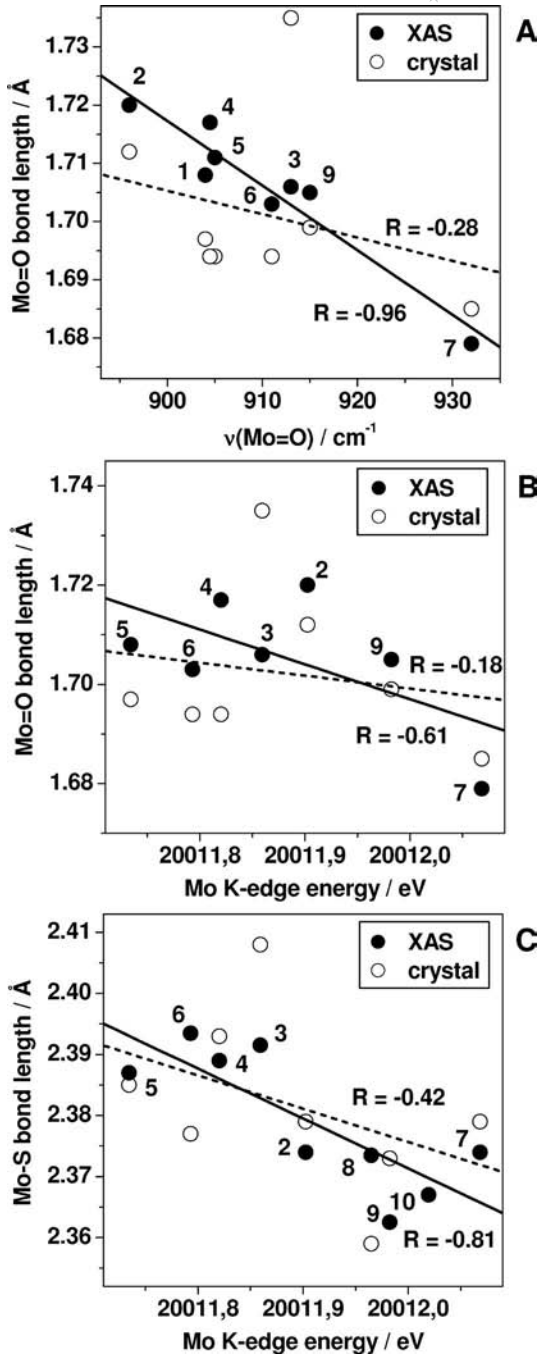

Figure 4. Relationships between Mo–ligand bond lengths, ν(Mo=O) from FTIR, and K-edge energies. Labels of data points denote **1** to **10** (distances from EXAFS, solid circles; distances from crystallography, open circles). The correlation coefficients (*R*) of linear regressions to respective data from EXAFS (solid lines) and crystallography (dashed lines) are indicated. EXAFS-derived parameters refer to best-fit data (lowest R_F values) in Table S1. Values for **1** were not included in the correlation analysis in (B) and (C) because of partial oxidation of the complex. Complex **10** is an exception in (A) and (B) because it does not carry an oxo ligand.

tion threshold energy (taken as the energy at edge half-height) reflects the onset of transitions to unoccupied antibonding orbitals of the metal–ligand σ bonds, which are at higher energies for more oxidized metals. Accordingly, the complexes with innocent sulfur-based ligands tend to contain molybdenum centers at a higher actual oxidation level. This is in agreement with shorter Mo=O bonds and higher ν(Mo=O) values, because the oxo ligand increases its electron donation into the Mo=O bond and the size of the metal center decreases with increased oxidation level. Interestingly, the Mo^{V} complex **9** exhibits an edge energy that is similar to that of Mo^{IV} compounds with no dithiolene ligands (**7** and **8**). This emphasizes not only the general non-innocent behavior of the dithiolene ligands with comparably low edge energies, but underlines the dramatically increased electron donation/redistribution to molybdenum in higher oxidation states. Molybdenum dithiolene complexes typically react to oxidation from the formal oxidation state IV to V with a change in the dithiolene folding angle; that is, the angle between the S–Mo–S and the S–C–C–S plane of the dithiolene moiety.[64–66] This is also reflected in **9**, in which the respective average folding angle of the bdt ligands is 20.65° from XRD. This is a considerable distortion from the more relaxed ligand geometry for instance in bis-bdt Mo^{IV} **1** with an average folding angle of 12.45° from XRD. This distortion allows a better overlap of the sulfur p orbital perpendicular to the C–S bond with a metal d orbital and facilitates electron donation on to the metal, effectively reducing the actual oxidation state of the metal. In the case of **9**, according to XAS edge energy analysis, the oxidation state is even reduced to a level at which it is more similar to Mo^{IV} than to Mo^{V} compounds. The immediate coordination sphere around molybdenum is not significantly influenced by this as it is very similar for **9** and Mo^{IV} compounds **1**–**8**.

The XANES spectra of **2**, **3**, **4**, and **5** from the dithiolene group show characteristic features, namely a pre-edge feature at ca. 20006.5 eV, an edge maximum at ca. 20036 eV, and a feature at ca. 20050 eV (Figure 5 top). The edge spectrum of **1** deviates due to partial oxidation of the sample. The distinct pre-edge feature, which is also present in the other five-coordinate molybdenum complexes, reflects dipole-forbidden 1s→4d electronic transitions, which gain intensity by p/d orbital mixing due to the short Mo=O bond causing a strong deviation from centrosymmetry. The XANES spectra of **6**, **7**, and **8** from the innocent sulfur donor group share a particularly pronounced shoulder at ca. 20020 eV in the edge rise, which is less intense in the case of **6** with a mixture of dithiolene and innocent ligand systems.

In order to understand and assign the distinct features of the near edge region in detail, XANES simulations were carried out on the model structures, which reproduce the experimental spectra well overall (Figure 5 top). Large deviations between experimental and calculated XANES spectra were observed only for **1** and **10**, which is in agreement with partial oxidation of **1** and partial replacement of Mo–CO by Mo=O in **10**, as concluded from the EXAFS

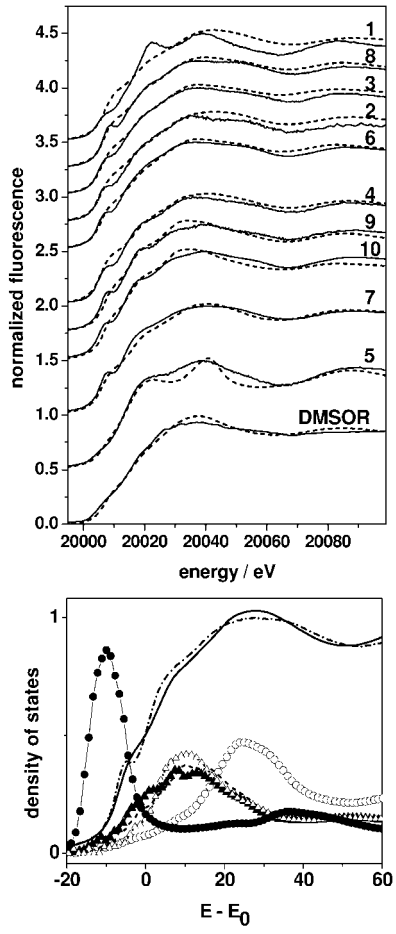

Figure 5. (Top) Mo K-edge spectra of model complexes and oxidized DMSOR. Solid lines, experimental data; dashed lines, calculated spectra. (Bottom) Experimental XANES of binuclear **9**, simulated spectrum (dash-dots) and calculated DOS of Mo–d (solid circles) and Mo–f (open circles) orbitals and of S–d orbitals for **3** (dashes), **7** (solid triangles), and **9** (open triangles).

analysis. The calculated number of unoccupied states at each energy, that is, the angular momentum projected density of states (DOS),[67] is related to the observed K-edge features, exemplified for **3**, **7**, and **9** in Figure 5 (bottom). The main edge peak is dominated by transitions into molybdenum f orbitals and the edge shoulder around 20020 eV mainly reflects transitions into orbitals with sulfur d character. Transitions into molybdenum d orbitals dominate the pre-edge features, as expected. The two bridging μ-S ligands in **9** cause a shift of the calculated S–d dominated transitions to lower energies, which is observed in the experimental spectrum (Figure 5 top and bottom). The sulfur d band calculated for the dithiolene sulfur atoms is similar for **3**, **6**, and **9**, but the influence of the more distant sulfur atoms of the S_4 ring in **6** and **7** modify the band shape. Accordingly, the edge shape reflects variations in both the first and second coordination spheres of molybdenum. The XANES spectrum of **10** shows only a small pre-edge feature due to its octahedral coordination geometry. A similar spectral shape is found for the six-coordinate molybdenum in

DMSOR (Figure 5 top), but here the edge energy is approximately 2 eV higher due to the presence of Mo^{VI}.

Discussion

In general, the structural features of the molybdenum centers (Mo^{IV} and Mo^{V} in **9**) observed in all the complexes investigated are remarkably similar, exhibiting a quite regular square-pyramidal geometry around molybdenum with the apical oxo moiety raised slightly above the S4 plane. This does not depend on whether dithiolenes or innocent sulfur donor ligands dominate the coordination environment. Accordingly, this geometry appears to be largely determined by the molybdenum ion itself.

The bis-mpt cofactor of reduced AO[45] has been described as being considerably distorted around the Mo^{IV} center, in which the four sulfur donors and the apical oxo ligand form an umbrella-shaped coordination sphere to expose the oxo function to a higher extent than in typical Moco models, some of which are part of this study. The distance between molybdenum and the S4 plane was reported to be approximately 0.8 Å in the enzyme.[45] This value, however, is not considerably larger than that observed in the model compounds in this study, the smallest value being 0.694 Å for binuclear **7**. The largest molybdenum S4–plane distance was 0.771 Å in **3**, which has to be taken with caution due to the disorder across the S4 plane. Trend wise, nonaromatic ligand systems (0.767 Å in **2** and 0.741 Å in **4**, for instance) allow a stronger distortion than aromatic ligands (0.717 Å in **5**). Overall the distortion observed in AO is, apparently, typical for the coordination environment of the Mo^{IV} center, without requiring any particular steric restraints through interaction with the peptide.

In accordance with previous XRD[60] and EXAFS data,[10,58–59] one of the four molybdenum(VI)–sulfur distances of DMSOR found in this study is significantly longer than the remaining three. This is because of the strong *trans* influence of the oxo ligand weakening the opposite metal–ligand bond. Again, this is chemically typical and supports the minor influence of the peptide environment on the active site geometry, which appears to be dominated by the molybdenum ion itself and steric restraints based on the dithiolene bite angle.

Both the Mo=O and the Mo–S bond lengths of the complexes with dithiolene ligands tend to be longer and the corresponding K-edge energies and ν(Mo=O) stretching frequencies are lower than those of the compounds with innocent sulfur donor ligands. Consequently, in the dithiolene complexes the metal has to be more reduced. Overall, this is surprisingly independent of the aromaticity of the dithiolene system even though small differences were observed (see above). In the compounds with innocent sulfur donor ligands, the apparent metal oxidation level was up to about half a unit higher. These findings underline the strong noninnocent character of the dithiolene-based ligands, which are able to donate considerable electron density not only into the metal–sulfur bond but, in extremes, onto the metal itself. This is most apparent in the data for the binuclear Mo^{V} complex **9**, which behaves in all aspects like the Mo^{IV}–dithiolene compounds and shows a K-edge energy very similar to those of the Mo^{IV} complexes without any dithiolene ligands (**7** and **8**).

With respect to XRD and absorption data, the results underline that structural analysis provides a more detailed three dimensional picture of the molecule investigated, resolving subtle differences in bond lengths and distortions of the dithiolene ligands. EXAFS, however, despite not being able to deliver the same resolution in bond length differences, appears to be more reliable with respect to metric parameters relevant (and in tune with other analytical results) for the bulk materials, because crystal packing forces do not interfere. In this study, this is particularly important regarding the molybdenum–oxo bond. A very reasonable correlation was found between the EXAFS Mo=O distance and the stretching vibration in the IR spectra. This particular correlation allows estimation of the length of the Mo=O bond by IR spectroscopy in the bulk material when the stretching vibration can be assigned unambiguously, at least in similar models. For cases in which crystal and IR data do not agree well, the specific correlation parameters determined by this study may prove useful. From another perspective, they may also help to avoid misleading assignment of IR vibrations.

The catalytic mechanism of Moco-dependent enzymes is based on the redox shuttling of the metal site between Mo^{IV}, Mo^{V}, and Mo^{VI} states. XANES analyses of bis-mpt containing DMSOR proteins and their mono-mpt pendants have revealed shifts of the K-edge by ca. 1 eV to higher energies per single electron oxidation of molybdenum,[63] indicating decidedly metal-centered oxidation. DFT calculations have corroborated this conclusion.[68] Thus, as has been pointed out earlier,[4] the molybdenum sites of the enzymes exhibit largely innocent behavior of the dithiolene-based ligands[54] in contrast to model compounds, despite their pronounced structural similarity.

In view of the variations in active site composition, for the particular reactivity neither the presence of one or two dithiolene units, nor of one or two oxygen ligands seems to be crucial, as members of distinct enzyme families can carry out the same catalytic reactions.[21,69–71] Apparently, the larger molybdenum environment is always fine-tuned so that ideal conditions with regard to the innocent vs. noninnocent character of mpt, metal-centered redox chemistry, and the exposure of the reactive site for substrate binding are obtained. Evidently, it is possible to model the immediate coordination sphere of molybdenum with respect to the geometry and most, if not all, ligand donor atoms. However, the inclusion of the pyran moiety into a model ligand does not allow sufficient electronic modeling of mpt, as the actual relative oxidation state of the respective model complex is much more similar to other simpler models than to the active sites of the enzymes. Structural motifs that could not be addressed by the model complexes used in this study include the pterin moiety of mpt, amino acid coordination to molybdenum (not relevant for AO and XO family), and

interactions of the active site with the protein matrix. Understanding exactly what contributes to the noninnocent behavior of the natural mpt ligand in the enzymes will require a substantial synthetic effort for the design of a new generation of model compounds addressing these structural motifs conclusively or step by step.

Furthermore, driving Moco and in particular mpt model chemistry further is a necessity and an important challenge with respect to possible ring opening at the pyran function of mpt and its potential roles in proton handling and electron guiding, which are still not adequately understood. As long as electronically and structurally accurate Moco models are not available, continuing research both on synthetic and natural systems is required to advance our understanding of the remarkable reactivity, specificity, and instability of molybdenum cofactors.

Experimental Section

Synthesis of Molybdenum Compounds: The model compounds were synthesized using Schlenk line techniques under a pure N_2 or Ar atmosphere. Solvents were predried for 2 d with KOH and heated to reflux for 3 d with calcium hydride, sodium/benzophenone or phosphorus pentoxide before distillation onto freshly regenerated molecular sieves with appropriate pore size. $K_3Na[MoO_2(CN)_4]\cdot 6H_2O$,[72] 4,5-dimetylbenzene-1,2-dithiol,[73] $[NEt_4]_2[MoO_2S_2]$,[74] $[Et_2NH_2]_2[MoOS_3]$,[75] $[NEt_4]_2[MoO(S_4)_2]$ (**7**),[75] 4,5-cyclohexano-[1,3]dithiol-2-one,[48] $[NEt_4]_2[MoO(bdt)_2]$ (**1**),[37] $[Mo(CO)_2(pdt)_2]$ (**10**),[42] $[NEt_4]_2[MoS(S_4)_2]$ (**8**),[43] and $[NEt_4]_2[Mo_2O_2(\mu\text{-}S)_2(bdt)_2]$ (**9**)[55] were synthesized according to literature procedures. For the known compounds $[NBzEt_3]_2[MoO(cydt)_2]$ (**2**),[42] $[PPh_4]_2[MoO(xdt)_2]$ (**3**),[21] and $[NEt_4]_2[MoO(tdt)_2]$ (**5**),[44,51–53] new and more economical procedures were developed. Other chemicals were purchased commercially and used as received. The three step synthesis of the ligand precursor for the preparation of $[NBu_4]_2[MoO(cdt)_2]$ (**4**) is outlined in the Supporting Information.

$[NBzEt_3]_2[MoO(cydt)_2]$ (2): 4,5-cyclohexano[1,3]dithiol-2-one (0.50 g, 2.90 mmol) was dissolved in MeOH (20 mL) and solid KOH (0.33 g, 5.80 mmol) was added. After 30 min stirring at 30 °C a color change to light yellow was observed. This mixture was added slowly at room temperature to a solution of $K_3Na[MoO_2(CN)_4]\cdot 6H_2O$ (0.77 g, 1.60 mmol) in water (20 mL). During addition, the color of the solution changed to red. The solution was stirred at 50 °C for 2 h. After cooling to room temperature, $BzNEt_3Cl$ (0.66 g, 2.90 mmol) dissolved in MeOH was added to the solution. To complete the reaction the mixture was stirred at room temperature for about 1 h. A dark red precipitate was observed. This product was dissolved in acetonitrile and dark red crystals were obtained by introducing several volumes of ether by vapor diffusion. Yield: 0.84 g (1.06 mmol, 67%). $C_{38}H_{60}MoN_2OS_4$ (784.30): calcd. C 58.13, H 7.70, N 3.57, S 16.34; found C 57.79, H 7.63, N 3.45, S 16.72. MS (FAB^+, 3-nitrobenzylalcohol) *m*/*z* (%) = 192.2 (100) [$BzNEt_3^+$]. MS (FAB^-, 3-nitrobenzylalcohol) *m*/*z* (%) = 401.9 (79). IR (KBr): $\tilde{\nu}$ = 502 (w), 537 (w), 669 (w), 679 (w), 705 (m), 751 (m), 804 (m), 878 (m), 880 (m), 1120 (m), 1154 (w), 1244 (s), 1313 (m), 1385 (m), 1466 (s), 1560 (w), 1597 (w), 1655 (m), 1624 (m), 1701 (w), 1719 (w), 2340 (w), 2345 (w), 2364 (w), 2854 (s), 2924 (vs), 3057 (w), 3204 (w) cm^{-1}. ^1H NMR (500 MHz, [D_6]DMSO, 25 °C, TMS): δ = 1.23 (t, ^3J = 2.7 Hz, 18 H, CH_3CH_2N), 1.76 (m, 8 H, cy*H*), 2.01 (m, 8 H, cy*H*), 2.41 (q, ^3J = 2.7 Hz, 12 H, CH_3CH_2N), 4.67 (br. m, 4 H, CH_2Ph), 7.07 (m, 2 H, H_{Arom}-NEt_3Bz), 7.57 (m, 4 H, $H_{Arom}NEt_3Bz$), 8.36 (m, 4 H, H_{Arom}-NEt_3Bz) ppm.

$[PPh_4]_2[MoO(xdt)_2]$ (3). Method A: $K_3Na[MoO_2(CN)_4]\cdot 6H_2O$ (0.86 g, 1.62 mmol) and NaOH (0.23 g, 5.87 mmol) were dissolved in H_2O (20 mL). To this solution was added 4,5-dimethylbenzene-1,2-dithiol (0.50 g, 2.94 mmol) in MeOH (20 mL) and a color change from blue to red was observed. The reaction mixture was heated to reflux for 20 min resulting in a dark red solution which was cooled and filtered before a solution of PPh_4Cl (1.10 g, 2.94 mmol) in MeOH (5 mL) was added. The reaction mixture was stirred for another hour at room temperature. Addition of H_2O (15 mL) resulted in the precipitation of an orange-brown solid. Purification was achieved by reprecipitation of the product from acetonitrile solution by addition of Et_2O by vapor diffusion. Yield: 0.63 g (0.56 mmol, 34%). $C_{64}H_{56}MoOP_2S_4$ (1126.21): calcd. C 68.19, H 5.01, S 11.38; found C 68.77, H 5.33, S 11.55. MS (FAB^+, 3-nitrobenzylalcohol) *m*/*z* (%) = 339.1 (100) [PPh_4^+]. MS (FAB^-, 3-nitrobenzylalcohol) *m*/*z* (%) = 450 (100) $[MoO(xdt)_2]^{2-}$. IR (KBr): $\tilde{\nu}$ = 446 (w), 526 (s), 691 (s), 724 (s), 756 (m), 804 (w), 874 (w), 913 (m), 996 (m), 1208 (w), 1108 (s), 1164 (w), 1187 (w), 1246 (m), 1314 (w), 1338 (w), 1374 (w), 1437 (s), 1482 (m), 1528 (w), 1584 (m), 1639 (m), 1774 (w), 1826 (w), 1910 (w), 2203 (w), 2690 (w), 2854 (w), 2914 (m), 2978 (w), 3052 (w) cm^{-1}. ^1H NMR (500 MHz, [D_6]DMSO, 25 °C, TMS): 2.49 (s, 12 H, CH_3), 7.18 (s, 4 H, H_{Arom}), 7.75 (m, 40 H, PCH_{Arom}) ppm. ^{13}C NMR (125.8 MHz, [D_6]-DMSO, 25 °C, TMS): 19.7 (CH_3), 118.2 (PC_{quart}), 118.9 (CH_{Arom}), 131.3 (CH*C*S), 131.4 (PC_{Arom}), 135.4 (PC_{Arom}), 135.5 (CCH_3), 136.2 (PC_{Arom}) ppm.

Method B: A solution of 4,5-dimethylbenzene-1,2-dithiol (0.12 g, 0.71 mmol) in acetonitrile (20 mL) was added to a solution of $[NEt_4]_2[MoO_2S_2]$ (0.16 g, 0.35 mmol) in acetonitrile (20 mL) with stirring at room temperature. The color of the solution changed immediately from orange to red. After 2 h, the solution was filtered. Storage of the solution at –35 °C afforded red/brown crystals after 10 d. Yield: 0.14 g (0.20 mmol, 56%). MS (FAB^+, 3-nitrobenzylalcohol) *m*/*z* (%) = 130.2 (100) [NEt_4^+]. MS (FAB^-, 3-nitrobenzylalcohol) *m*/*z* (%) = 449.9 (100) $[MoO(xdt)_2]^{2-}$. IR (KBr): $\tilde{\nu}$ = 507 (m), 555 (w), 640 (w), 713 (w), 746 (w), 805 (w), 870 (w), 985 (m), 1155 (s), 1209 (s), 1241 (s), 1310 (m), 1385 (w), 1457 (w), 1474 (w), 1541 (w), 1636 (w), 2282 (w), 2389 (w), 2855 (w), 2926 (w), 2967 (w) cm^{-1}. ^1H NMR (300 MHz, [D_6]DMSO, 25 °C, TMS): 1.05 (*t*, ^3J = 6.0 Hz, 24 H, CH_3CH_2), 2.13 (s, 12 H, CH_3), 2.80 (*q*, ^3J = 6.0 Hz, 16 H, CH_3CH_2), 7.13 (s, 4 H, H_{Arom}) ppm. ^{13}C NMR (75.47 MHz, [D_6]DMSO, 25 °C, TMS): 7.0 (CH_3CH_2), 18.9 (CH_3C_{Arom}), 51.3 (CH_2CH_3), 127.5 (CH_{Arom}), 128.7 (CH*C*S), 147.6 (CCH_3) ppm.

$[NBu_4]_2[MoO(cdt)_2]$ (4): 4H-[1,3]dithiolo[4,5-*c*]chromen-2-one (0.38 g, 1.71 mmol; for preparation see the Supporting Information) was dissolved in oxygen-free methanol (12.5 mL) and stirred for 45 min with KOH (0.38 g, 6.83 mmol). The solution immediately turned dark reddish brown and to this a blue solution of $K_3Na[MoO_2(CN)_4]\cdot 6H_2O$ (0.41 g, 0.85 mmol) in oxygen-free water was added under a nitrogen atmosphere. The reaction mixture was stirred for 3 h at 70 °C, cooled, and the solvents were removed in vacuo. The remaining solid was then dissolved in water (10 mL) and washed three times with oxygen-free chloroform to remove the organic compounds. The aqueous layer was collected, dried, dissolved in oxygen-free acetonitrile and filtered. Evaporation of acetonitrile in vacuo afforded a red solid. The product was dissolved again in oxygen-free water (20 mL) and a solution of NBu_4Br (0.55 g, 1.71 mmol) in water (20 mL) was added dropwise with constant stirring. The precipitated orange-brown compound was fil-

tered, washed with water, and dried in vacuo overnight. Yield: 0.30 g (0.31 mmol, 36%). $C_{50}H_{84}MoN_2O_3S_4$ (948.48): calcd. C 60.94, H 8.59, N 2.84, S 13.02; found C 60.80, H 8.53, N 2.88, S 12.89. MS (FAB$^-$, 3-nitrobenzylalcohol) *m/z* (%) = 501.9 $[MoO(cdt)_2]^{2-}$. IR (KBr): $\tilde{\nu}$ = 448.1 (w), 482.1 (w), 519.6 (w), 547.5 (w), 618.2 (w), 643.0 (m), 749.6 (s), 784.0 (m), 904.5 (s), 993.2 (m), 1033.5 (m), 1065.4 (w), 1084.9 (w), 1107.2 (w), 1150.0 (w), 1215.7 (m), 1246.6 (m), 1303.5 (w), 1359.5 (w), 1380.6 (m), 1479.0 (s), 1550.5 (m), 1577.4 (m), 2443.9 (w), 2703.7 (w), 2816.8 (w), 2874.1 (m), 2939.2 (s), 2961.3 (s), 3023.4 (w), 3065.9 (w) cm^{-1}. ^{1}H NMR (CD_3CN, 500 MHz): 7.86–7.82 (m, 2 H, CH_{Arom}), 6.87 (m, 4 H, CH_{Arom}), 6.74 (m, 2 H, CH_{Arom}), 5.10 (s, 4 H, OCH_2), 2.97–2.94 (t, 16 H, NCH_2CH$_3$), 1.45–1.39 (p, 16 H, CH$_2$CH_2CH$_2$), 1.30–1.22 (h, 16 H, CH$_2$CH_2CH$_3$), 0.88–0.85 (t, 24 H, CH_2CH$_3$). ^{13}C NMR (CD_3CN, 125.8 MHz, 25 °C, TMS): 13.89 (*C*H$_3$), 20.32 (*C*H$_2$CH$_3$), 24.36 (CH$_2$*C*H$_2$CH$_2$), 58.97 (N*C*H$_2$), 74.14 (O*C*H$_2$), 114.60 (*C*H$_{Arom}$), 118.254 (*C*H$_{Arom}$), 121.505 (S*C*), 124.49 (*C*H$_{Arom}$), 125.76 (*C*H$_{Arom}$), 152.10 (O*C*).

$[NEt_4]_2[MoO(tdt)_2]$ (5): Toluene-3,4-dithiol (0.30 g, 1.92 mmol) was dissolved in EtOH (20 mL) and added slowly to a solution of $K_3Na[MoO_2(CN)_4]\cdot 6H_2O$ (0.52 g, 1.08 mmol) dissolved in oxygen-free water (20 mL) at room temperature. A color change from blue to red was observed. After one hour stirring at room temperature NEt_4Br (0.44 g, 2.09 mmol) was added to the mixture. The formation of a dark red precipitate was observed and the compound was collected by filtration. The solid was washed five times with ethanol (5 mL). After removing all solvents in vacuo the product was recrystallized from acetonitrile/diethyl ether (1:1). After 3 d orange-red crystals were formed at –35 °C. Yield: 0.48 g (0.70 mmol, 65%). $C_{30}H_{52}MoN_2OS_4$ (680.24): calcd. C 52.91, H 7.70, N 4.11, S 18.84; found C 52.66, H 7.44, N 3.88, S 18.66. MS (ESI$^+$, MeOH) *m/z* (%) = 130.2 (80) $[NEt_4^+]$, 682.3 $[NEt_4]_2[MoO(tdt)_2]$; MS (ESI$^-$, MeOH) *m/z* (%) = 422 (65) $[MoO(tdt)_2]^{2-}$. MS (FAB$^-$, 3-nitrobenzylalcohol) *m/z* (%) = 422 (80) $[MoO(tdt)_2]^{2-}$. IR (KBr): $\tilde{\nu}$ = 418 (w), 440 (w), 471 (w), 507 (w), 556 (w), 648 (w), 669 (w), 679 (w), 686 (w), 714 (w), 808 (s), 839 (s), 860 (s), 904 (s), 984 (m), 999 (m), 1052 (w), 1092 (m), 1128 (w), 1154 (w), 1172 1242 (vs), 1310 (m), 1392 (m), 1448 (s), 1481 (s), 1541 (w), 1559 (w), 1576 (w), 1654 (w), 1701 (w), 1718 (w), 1734 (w), 1793 (w), 2083 (w), 2340 (m), 2343 (m), 2343 (m), 2361 (m), 2858 (w), 2918 (w), 2976 (m), 3179 (w) cm^{-1}.

$[NEt_4]_2[MoO(xdt)(S_4)]$ (6): To a solution of $[NEt_4]_2[MoO(S_4)_2]$ (500 mg, 0.795 mmol) in acetonitrile (50 mL) was added a solution of 4,5-dimethylbenzene-1,2-dithiol (0.14 g, 0.795 mmol) in acetonitrile (20 mL) at room temperature. The solution was stirred at room temperature for 5 h. After reducing the volume of the solution to around 40 mL, a yellow precipitate was formed, which proved to be elemental sulfur. After filtration the solution was stored at –30 °C and another batch of yellow sulfur formed. From the filtrate red brown crystals were formed by vapor diffusion with diethyl ether and acetonitrile. Yield: 368 mg (0.574 mmol; 72%). $C_{24}H_{48}MoN_2OS_6$ (668.15): calcd. C 43.09, H 7.23, N 4.19, S 28.76; found C 43.75, H 7.95, N 4.35, S 29.64. MS [ESI$^+$, MeOH] *m/z* (%) = 130.2 (100) $[NEt_4^+]$. MS [ESI$^-$, MeOH] *m/z* (%) = 409.3 (11) $[MoO(xdt)(S)_4]^{2-}$. IR (KBr): $\tilde{\nu}$ = 419 (w), 440 (w), 505 (w), 555 (w), 640 (w), 679 (w), 711 (w), 747 (w), 784 (m), 802 (w), 867 (w), 911 (m), 931 (m), 985 (m), 1156 (s), 1210 (s), 1241 (vs), 1310 (s), 1363 (m), 1389 (m), 1447 (m), 1479 (m), 1654 (w), 2340 (w), 2345 (w), 2361 (w), 2930 (w), 2972 (w) cm^{-1}. ^{1}H NMR (300 MHz, [D$_6$] DMSO, 25 °C, TMS): 1.07 (*t*, ^3J = 6.0 Hz, 24 H, CH_3CH$_2$), 2.26 (s, 6 H, CH_3), 2.85 (*q*, ^3J = 6.0 Hz, 16 H, CH$_3$CH_2), 7.18 (s, 4 H, H$_{Arom}$) ppm.

X-ray Crystallography: Suitable crystals were mounted on a glass fiber and data were collected with an IPDS II Stoe image-plate diffractometer [graphite monochromated molybdenum K_α radiation, λ = 0.71073 Å at 133(2) K]. The data were integrated with X-Area. The structures were solved by direct methods (SHELXS-97) [76] and refined by full-matrix least square methods against F^2 (SHELXL-97).[76] All non-hydrogen atoms were refined with anisotropic displacement parameters. The hydrogen atoms were attached at idealized positions on carbon atoms and were refined as riding atoms with uniform isotropic thermal parameters except for the disordered TEA cations. Here the hydrogen atoms on the methyl groups, which are formally bound to two disordered methylene groups, were either refined when found or not refined at all. The crystallographic data collection and refinement parameters for the four new X-ray structures are summarized in Table 3. CCDC-782750 (for **2**), -782752 (for **4**), -782753 (for **5**), and -782751 (for **6**) contain the supplementary crystallographic data for this paper. These data can be obtained free of charge from The Cam-

Table 3. Crystallographic data for the structural analyses of $[NBzEt_3]_2\cdot$**2**, $[NBu_4]_2\cdot$**4**, $[NEt_4]_2\cdot$**5**, and $[NEt_4]_2\cdot$**6**.

	$[NBzEt_3]_2\cdot$**2**	$[NBu_4]_2\cdot$**4**	$[NEt_4]_2\cdot$**5**	$[NEt_4]_2\cdot$**6**
Empirical formula	$C_{38}H_{60}MoON_2S_4$	$C_{50}H_{84}MoN_2O_3S_4$	$C_{30}H_{52}MoN_2OS_4$	$C_{24}H_{48}MoN_2OS_6$
T /K	133(2)	133(2)	133(2)	133(2)
Crystal system	monoclinic	monoclinic	monoclinic	monoclinic
Space group	$P2_1/c$	Cc	$P2_1$	$P2_1/n$
a /Å	10.513(2)	15.815(3)	9.2242(18)	15.956(3)
b /Å	22.232(4)	20.813(4)	13.834(3)	12.071(3)
c /Å	17.823(4)	16.284(3)	13.307(3)	17.111(3)
β /°	103.65(3)	105.03(3)	97.69(3)	109.01(3)
V /Å^3	4048.1(14)	5176.7(18)	1682.9(6)	3115.9(11)
Z	4	4	2	4
D_{calc} /g cm^{-3}	1.288	1.264	1.348	1.426
μ /mm^{-1}	0.561	0.455	0.663	0.843
F(000)	1664	2112	724	1408
θ range /°	1.49–25.92	1.65–27.16	1.54–26.96	1.52–27.07
Data/ restraints/ parameters	7817/6/405	10506/5/525	6915/13/282	6805/0/307
Reflections collected/unique (R_{int})	31651/7817 (0.0741)	24985/10506 (0.1130)	15217/6915 (0.0338)	27529/6805 (0.1219)
*R*1, *wR*$_2$ [$I>2\sigma(I)$][a]	0.0443, 0.1148	0.0812, 0.1357	0.0540, 0.1400	0.0383, 0.0739
*R*1, *wR*$_2$ (all data)[a]	0.0594, 0.1208	0.1379, 0.1559	0.0546. 0.1405	0.0568, 0.0785
GoF	1.059	1.047	1.049	0.950
$\Delta\rho$(max), $\Delta\rho$(min) /e Å^{-3}	0.897, –1,142	0.751, –0.451	1.485, –0.883	0.722, –0.807

[a] $R1 = \Sigma||F_o| - |F_c||/\Sigma|F_o|$. $wR_2 = [\Sigma w(F_o^2 - F_c^2)^2/\Sigma w(F_o^2)^2]^{0.5}$.

bridge Crystallographic Data Centre via www.ccdc.cam.ac.uk/data_request/cif.

Protein Sample Preparation: *Rhodobacter sphaeroides* DMSOR from plasmid pJH720 was expressed in a heterologous expression system in *Escherichia coli* MG1655 cells and purified by Ni-NTA affinity chromatography as described by Hilton et al.[77] The protein in tris(hydroxymethyl)aminomethane buffer (100 mM, pH 7.2) was concentrated to ca. 2 mM (Centricon, Millipore), filled into sample holders for XAS, and stored in liquid nitrogen.

X-ray Absorption Spectroscopy (XAS): Samples of model complexes were pelletized in polyethylene (ca. 10%) prepared under an inert gas atmosphere. XAS at the Mo K-edge was performed at the synchrotron SOLEIL (Paris, France) at the SAMBA beamline using a double crystal (Si220) monochromator for scanning of the excitation energy and two palladium-coated mirrors in grazing incidence mode for focusing the X-ray beam (spot size ca. 2.5×1 mm^2) and for harmonics rejection. The energy axis was calibrated (accuracy ± 0.1 eV) using the first inflection point at 20003.9 eV in the simultaneously measured absorption spectrum of a Mo foil as a standard. Fluorescence-detected XAS spectra were measured using an energy resolving 7-element solid state Ge detector (Canberra), which was shielded by 10 μm Zr foil against scattered X-rays. The total incoming count-rate was kept well below 20000 s^{-1} to avoid detector saturation. Samples were held in a liquid helium cryostat at 20 K. XAS spectra (scan range of 19850–21050 eV, i.e. up to k = 16 Å^{-1}); two scans per sample spot were corrected for detector dead time and averaging (4–8 spots per sample), normalization, and extraction of EXAFS oscillations and conversion of the energy scale to the wave-vector scale (k-scale) was performed as described previously.[78] k^3-weighted EXAFS spectra were simulated (S_0^2 = 1.0) by a least-squares procedure using phase functions calculated with FEFF7[79] and FTs were calculated using the in-house software SimX.[80–81] E_0 refined to 20008 ± 3 eV in the fit procedure. The fit quality was judged by calculation of the Fourier-filtered R-factor (R_F).[82] The pre-edge structure of XANES spectra was isolated by subtracting a polynomial spline from the main K-edge rise using the software XANDA.[83] K-edge energies denote values at 50% of normalized edge absorption (edge half-height).

XANES Simulation: K-edge spectra were calculated using FEFF9[84–85] with the full multiple scattering and self consistent field parameters activated. Values of the ionization card of 1.2 for Mo and of –0.4 for O and S ligands were used. The amplitude reduction factor S_0^2 was calculated by the FEFF program. Input files with atomic coordinates of model structures were generated using HyperChem. (Hypercube) on the basis of crystal structures for complexes **2**, **3**, **4**, **5**, **6**, and **9**. For **1** the structure of **3** and for **7** and **8** the structure of **6** was used as a template and respective model structures included the Mo–ligand distances from EXAFS analysis. The model of **10** was built using EXAFS-derived bond lengths only.

NMR, FTIR, and Mass Spectrometry Measurements: NMR spectra were recorded using Bruker Avance DRX 500 or Bruker Avance DPX 300 spectrometers. The residual ^{1}H or ^{13}C peak of the deuteriated solvent was used as an internal standard and tetramethylsilane as external standard for ^{1}H spectra. IR spectra were collected with a Mattson Genesis FT-MIR spectrometer in the range of 400–4000 cm^{-1} as KBr pellets. Mass spectra were recorded with a Finnigan MAT System 8200. For FAB spectra ionization was achieved using 3-nitrobenzylalcohol. Elemental analyses were carried out with a 4.1 Varido EL 3 Analyzer from Elementar.

Supporting Information (see footnote on the first page of this article): Synthesis of organic precursors of **4**; EXAFS simulation parameters.

Acknowledgments

P. P. S. and C. S. would like to thank the Deutsche Forschungsgemeinschaft (DFG) for generous financial support (IRTG1422 and SCH1480/3-2). K. G. V. H. thanks the "Bengt Lundqvist Minne" and the Wenner–Gren Foundation for fellowships. M. H. thanks the Deutsche Forschungsgemeinschaft (DFG) for a Heisenberg Fellowship and for funding (Ha3265/3–1). M. H. and S. L. were supported by project B3 of the Unicat Cluster of Excellence (Berlin). We thank Dr. E. Fonda at the Samba beamline at SOLEIL for excellent technical support.

[1] R. Hille, *Chem. Rev.* **1996**, *96*, 2757–2816.
[2] M. K. Johnson, D. C. Rees, M. W. Adams, *Chem. Rev.* **1996**, *96*, 2817–2840.
[3] R. Hille, *Trends Biochem. Sci.* **2002**, *27*, 360–367.
[4] J. H. Enemark, J. J. Cooney, J. J. Wang, R. H. Holm, *Chem. Rev.* **2004**, *104*, 1175–1200.
[5] L. E. Bevers, P. L. Hagedoorn, W. R. Hagen, *Coord. Chem. Rev.* **2009**, *253*, 269–290.
[6] K. V. Rajagopalan, J. L. Johnson, *J. Biol. Chem.* **1992**, *267*, 10199–10202.
[7] S. Leimkühler, M. M. Wuebbens, K. V. Rajagopalan, *Coord. Chem. Rev.* **2011**, *255*, 1129–1144.
[8] C. Kisker, H. Schindelin, D. Baas, J. Retey, R. U. Meckenstock, P. M. H. Kroneck, *Fems Microbiol. Rev.* **1998**, *22*, 503–521.
[9] M. J. Romao, *Dalton Trans.* **2009**, 4053–4068.
[10] G. N. George, *J. Biol. Inorg. Chem.* **1997**, *2*, 790–796.
[11] L. J. Laughlin, A. A. Eagle, G. N. George, E. R. Tiekink, C. G. Young, *Inorg. Chem.* **2007**, *46*, 939–948.
[12] C. J. Doonan, N. D. Rubie, K. Peariso, H. H. Harris, S. Z. Knottenbelt, G. N. George, C. G. Young, M. L. Kirk, *J. Am. Chem. Soc.* **2008**, *130*, 55–65.
[13] C. J. Doonan, H. L. Wilson, K. V. Rajagopalan, R. M. Garrett, B. Bennett, R. C. Prince, G. N. George, *J. Am. Chem. Soc.* **2007**, *129*, 9421–9428.
[14] G. N. George, K. J. Nelson, H. H. Harris, C. J. Doonan, K. V. Rajagopalan, *Inorg. Chem.* **2007**, *46*, 3097–3104.
[15] G. N. George, C. J. Doonan, R. A. Rothery, N. Boroumand, J. H. Weiner, *Inorg. Chem.* **2007**, *46*, 2–4.
[16] C. J. Doonan, U. Kappler, G. N. George, *Inorg. Chem.* **2006**, *45*, 7488–7492.
[17] C. J. Doonan, A. Stockert, R. Hille, G. N. George, *J. Am. Chem. Soc.* **2005**, *127*, 4518–4522.
[18] G. N. George, R. M. Garrett, R. C. Prince, K. V. Rajagopalan, *Inorg. Chem.* **2004**, *43*, 8456–8460.
[19] G. N. George, C. M. Colangelo, J. Dong, R. A. Scott, S. V. Khangulov, V. N. Gladyshev, T. C. Stadtman, *J. Am. Chem. Soc.* **1998**, *120*, 1267–1273.
[20] P. E. Baugh, C. D. Garner, J. M. Charnock, D. Collison, E. S. Davies, A. S. McAlpine, S. Bailey, I. Lane, G. R. Hanson, A. G. McEwan, *J. Biol. Inorg. Chem.* **1997**, *2*, 634–643.
[21] K. G. Havelius, S. Reschke, S. Horn, A. Döring, D. Niks, R. Hille, C. Schulzke, S. Leimkuhler, M. Haumann, *Inorg. Chem.* **2011**, *50*, 741–748.
[22] R. K. Szilagyi, B. S. Lim, T. Glaser, R. H. Holm, B. Hedman, K. O. Hodgson, E. I. Solomon, *J. Am. Chem. Soc.* **2003**, *125*, 9158–9169.
[23] A. L. Tenderholt, R. K. Szilagyi, R. H. Holm, K. O. Hodgson, B. Hedman, E. I. Solomon, *Inorg. Chem.* **2008**, *47*, 6382–6392.
[24] R. Sarangi, S. DeBeer George, D. J. Rudd, R. K. Szilagyi, X. Ribas, C. Rovira, M. Almeida, K. O. Hodgson, B. Hedman, E. I. Solomon, *J. Am. Chem. Soc.* **2007**, *129*, 2316–2326.

[25] P. Banerjee, S. Sproules, T. Weyhermüller, S. DeBeer George, K. Wieghardt, *Inorg. Chem.* **2009**, *48*, 5829–5847.
[26] R. Kapre, K. Ray, I. Sylvestre, T. Weyhermüller, S. DeBeer George, F. Neese, K. Wieghardt, *Inorg. Chem.* **2006**, *45*, 3499–3509.
[27] K. Ray, S. DeBeer George, E. I. Solomon, K. Wieghardt, F. Neese, *Eur. J. Inorg. Chem.* **2007**, *13*, 2783–2797.
[28] J. S. Pap, F. L. Benedito, E. Bothe, E. Bill, S. DeBeer George, T. Weyhermüller, K. Wieghardt, *Inorg. Chem.* **2007**, *46*, 4187–4196.
[29] R. R. Kapre, E. Bothe, T. Weyhermüller, S. DeBeer George, K. Wieghardt, *Inorg. Chem.* **2007**, *46*, 5642–5650.
[30] R. R. Kapre, E. Bothe, T. Weyhermüller, S. DeBeer George, N. Muresan, K. Wieghardt, *Inorg. Chem.* **2007**, *46*, 7827–7839.
[31] S. Sproules, F. L. Benedito, E. Bill, T. Weyhermüller, S. DeBeer George, K. Wieghardt, *Inorg. Chem.* **2009**, *48*, 10926–10941.
[32] C. Milsmann, G. K. Patra, E. Bill, T. Weyhermüller, S. DeBeer George, K. Wieghardt, *Inorg. Chem.* **2009**, *48*, 7430–7445.
[33] C. Milsmann, E. Bill, T. Weyhermüller, S. DeBeer George, K. Wieghardt, *Inorg. Chem.* **2009**, *48*, 9754–9766.
[34] S. Sproules, T. Weyhermüller, S. DeBeer, K. Wieghardt, *Inorg. Chem.* **2010**, *49*, 5241–5261.
[35] K. Peariso, M. E. Helton, E. N. Duesler, S. E. Shadle, M. L. Kirk, *Inorg. Chem.* **2007**, *46*, 1259–1267.
[36] H. Sugimoto, M. Tarumizu, K. Tanaka, H. Miyake, H. Tsukube, *Dalton Trans.* **2005**, 3558–3565.
[37] S. Boyde, S. R. Ellis, C. D. Garner, W. Clegg, *J. Chem. Soc., Chem. Commun.* **1986**, 1541–1543.
[38] K. Baba, T. A. Okamura, C. Suzuki, H. Yamamoto, T. Yamamoto, M. Ohama, N. Ueyama, *Inorg. Chem.* **2006**, *45*, 894–901.
[39] B. S. Lim, R. H. Holm, *J. Am. Chem. Soc.* **2001**, *123*, 1920–1930.
[40] K. B. Musgrave, B. S. Lim, K. M. Sung, R. H. Holm, B. Hedman, K. O. Hodgson, *Inorg. Chem.* **2000**, *39*, 5238–5247.
[41] A. L. Tenderholt, J. J. Wang, R. K. Szilagyi, R. H. Holm, K. O. Hodgson, B. Hedman, E. I. Solomon, *J. Am. Chem. Soc.* **2010**, *132*, 8359–8371.
[42] H. Sugimoto, M. Harihara, M. Shiro, K. Sugimoto, K. Tanaka, H. Miyake, H. Tsukube, *Inorg. Chem.* **2005**, *44*, 6386–6392.
[43] M. Draganjac, E. Simhon, L. T. Chan, M. Kanatzidis, N. C. Baenziger, D. Coucouvanis, *Inorg. Chem.* **1982**, *21*, 3321–3332.
[44] H. Oku, N. Ueyama, M. Kondo, A. Nakamura, *Inorg. Chem.* **1994**, *33*, 209–216.
[45] P. J. Ellis, T. Conrads, R. Hille, P. Kuhn, *Structure* **2001**, *9*, 125–132.
[46] T. Conrads, C. Hemann, G. N. George, I. J. Pickering, R. C. Prince, R. Hille, *J. Am. Chem. Soc.* **2002**, *124*, 11276–11277.
[47] G. Periyasamy, N. A. Burton, I. H. Hillier, M. A. Vincent, H. Disley, J. McMaster, C. D. Garner, *J. Chem. Soc. Faraday Trans.* **2007**, *135*, 469–488.
[48] A. K. Bhattacharya, A. G. Hortmann, *J. Org. Chem.* **1974**, *39*, 95–97.
[49] A. K. Bhattacharya, A. G. Hortmann, *Int. J. Sulfur Chem.* **1973**, *8*, 273–278.
[50] E. S. Davies, R. L. Beddoes, D. Collison, A. Dinsmore, A. Docrat, J. A. Joule, C. R. Wilson, C. D. Garner, *J. Chem. Soc., Dalton Trans.* **1997**, 3985–3995.
[51] A. T. Pilipenko, V. V. Trachevskii, N. V. Rusetskaya, *Zh. Neorg. Khim.* **1979**, *24*, 1253–1261.
[52] P. C. H. Mitchell, C. F. Pygall, *Inorg. Chim. Acta* **1979**, *33*, L109–L111.
[53] N. Ueyama, H. Oku, M. Kondo, T. Okamura, N. Yoshinaga, A. Nakamura, *Inorg. Chem.* **1996**, *35*, 643–650.
[54] F. J. Hine, A. J. Taylor, C. D. Garner, *Coord. Chem. Rev.* **2010**, *254*, 1570–1579.
[55] A. Döring, C. Schulzke, Q. W. Zhang, *Inorg. Chim. Acta* **2010**, *363*, 4140–4144.
[56] U. Ryde, C. Schulzke, K. Starke, *J. Biol. Inorg. Chem.* **2009**, *14*, 1053–1064.
[57] N. Ueyama, H. Oku, A. Nakamura, *J. Am. Chem. Soc.* **1992**, *114*, 7310–7311.
[58] G. N. George, J. Hilton, C. Temple, R. C. Prince, K. V. Rajagopalan, *J. Am. Chem. Soc.* **1999**, *121*, 1256–1266.
[59] G. N. George, J. Hilton, K. V. Rajagopalan, *J. Am. Chem. Soc.* **1996**, *118*, 1113–1117.
[60] H. Schindelin, C. Kisker, J. Hilton, K. V. Rajagopalan, D. C. Rees, *Science* **1996**, *272*, 1615–1621.
[61] F. Schneider, J. Lowe, R. Huber, H. Schindelin, C. Kisker, J. Knablein, *J. Mol. Biol.* **1996**, *263*, 53–69.
[62] A. S. McAlpine, A. G. McEwan, S. Bailey, *J. Mol. Biol.* **1998**, *275*, 613–623.
[63] G. N. George, C. A. Kipke, R. C. Prince, R. A. Sunde, J. H. Enemark, S. P. Cramer, *Biochemistry* **1989**, *28*, 5075–5080.
[64] J. W. Lauher, R. Hoffmann, *J. Am. Chem. Soc.* **1976**, *98*, 1729–1742.
[65] H. K. Joshi, J. H. Enemark, *J. Am. Chem. Soc.* **2004**, *126*, 11784–11785.
[66] J. J. A. Cooney, M. A. Cranswick, N. E. Gruhn, H. K. Joshi, J. H. Enemark, *Inorg. Chem.* **2004**, *43*, 8110–8118.
[67] G. A. Simms, J. D. Padmos, P. Zhang, *J. Chem. Phys.* **2009**, *131*, 214703.
[68] H. H. Harris, G. N. George, K. V. Rajagopalan, *Inorg. Chem.* **2006**, *45*, 493–495.
[69] K. Fischer, G. G. Barbier, H. J. Hecht, R. R. Mendel, W. H. Campbell, G. Schwarz, *Plant Cell* **2005**, *17*, 1167–1179.
[70] J. M. Dias, M. E. Than, A. Humm, R. Huber, G. P. Bourenkov, H. D. Bartunik, S. Bursakov, J. Calvete, J. Caldeira, C. Carneiro, J. J. Moura, I. Moura, M. J. Romao, *Structure* **1999**, *7*, 65–79.
[71] W. Clegg, G. Christou, C. D. Garner, G. M. Sheldrick, *Inorg. Chem.* **1981**, *20*, 1562–1566.
[72] A. Roodt, S. S. Basson, J. G. Leipoldt, *Polyhedron* **1994**, *13*, 599–607.
[73] E. Klingsberg, *Synth. Int. J. Methods* **1972**, 29.
[74] J. W. Mcdonald, G. D. Friesen, L. D. Rosenhein, W. E. Newton, *Inorg. Chim. Acta* **1983**, *72*, 205–210.
[75] M. A. Ansari, J. Chandrasekaran, S. Sarkar, *Inorg. Chim. Acta* **1987**, *133*, 133–136.
[76] G. M. Sheldrick, *Acta Crystallogr., Sect. A* **2008**, *64*, 112–122.
[77] J. C. Hilton, C. A. Temple, K. V. Rajagopalan, *J. Biol. Chem.* **1999**, *274*, 8428–8436.
[78] H. Dau, P. Liebisch, M. Haumann, *Anal. Bioanal. Chem.* **2003**, *376*, 562–583.
[79] J. J. Rehr, J. M. Deleon, S. I. Zabinsky, R. C. Albers, *J. Am. Chem. Soc.* **1991**, *113*, 5135–5140.
[80] J. Dittmer, *Linear-Dichroismus-Röntgenabsorptionsspektroskopie zum katalytischen Zyklus des wasserspaltenden Mangankomplexes der Photosynthese in Theorie und Experiment*, Christian-Albrechts Universität, Kiel, **1999**.
[81] H. Dau, P. Liebisch, M. Haumann, *Phys. Chem. Chem. Phys.* **2004**, *6*, 4781–4792.
[82] C. Meinke, V. A. Sole, P. Pospisil, H. Dau, *Biochemistry* **2000**, *39*, 7033–7040.
[83] K. V. Klementiev, XANES dactyloscope for Windows. www.desy.de/~klmn/xanda.html.
[84] R. M. van der Veen, J. J. Kas, C. J. Milne, V. T. Pham, A. El Nahhas, F. A. Lima, D. A. Vithanage, J. J. Rehr, R. Abela, M. Chergui, *Phys. Chem. Chem. Phys.* **2010**, *12*, 5551–5561.
[85] J. J. Rehr, J. J. Kas, F. D. Vila, M. P. Prange, K. Jorissen, *Phys. Chem. Chem. Phys.* **2010**, *12*, 5503–5513.

Received: March 29, 2011
Published Online: August 19, 2011

